ACS APPLIED MATERIALS & INTERFACES

LETTER

www.acsami.org

Aqueous-Solution-Processed Hybrid Solar Cells from Poly(1,4-naphthalenevinylene) and CdTe Nanocrystals

Zhanxi Fan, Hao Zhang, Weili Yu, Zhenyu Xing, Haotong Wei, Qingfeng Dong, Wenjing Tian, and Bai Yang*

State Key Laboratory of Supramolecular Structure and Materials, College of Chemistry, Jilin University, Changchun 130012, People's Republic of China

ABSTRACT: Poly(1,4-naphthalenevinylene), prepared from a water-soluble precursor, was used to fabricate hybrid solar cells by blending with water-soluble CdTe nanocrystals (NCs) to act as the photoactive layer. In composites with CdTe NCs as the electron acceptors in a bulk heterojunction configuration, the devices exhibited a short-circuit current density of −6.14 mA/cm^2, an open-circuit voltage of 0.44 V, a fill factor of 0.32, and a power conversion efficiency of 0.86% under AM1.5G conditions. Because the devices were fabricated from water-soluble materials, the procedure was generally simple and environmentally friendly in comparison to the conventional devices fabricated from oil-soluble materials.

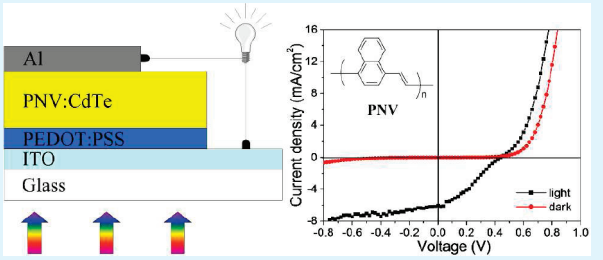

KEYWORDS: hybrid solar cells, aqueous solution processed, bulk heterojunction, conjugated polymers, inorganic nanocrystals

INTRODUCTION

With respect to renewable energy, π-conjugated polymer-based plastic solar cells (π-PSCs) have recently been considered as alternatives to conventional inorganic solar cells because of the advantages of ease of processing, low cost, lightweightedness, large area, as well as mechanical flexibility.[1−5] π-PSCs are mainly constructed in a bulk heterojunction (BHJ) configuration in which the domain sizes of the donors and acceptors are comparable with the exciton diffusion length so as to maximize the exciton dissociation efficiency.[6,7] However, the power conversion efficiency (PCE) of π-PSCs is limited by the poor absorption of fullerene derivatives, low mobility of charge carriers, and so forth. One promising effort to solve this problem is the use of semiconductor nanocrystals (NCs) as acceptors to fabricate hybrid solar cells (HSCs), which leads to high absorption coefficients, high electron mobility, and feasibility of adjusting the band gap by varying the NC size.[8]

NC−polymer HSCs have been extensively studied since the pioneering work of Wang and Herron[9] and Alivisatos and coworkers.[10] So far, there are four kinds of π-conjugated polymers that have been involved in HSCs as the donor materials: poly(phenylenevinylene) derivatives (such as OC_1C_{10}-PPV[11] and MEH-PPV[12]), polythiophene derivatives (such as P3HT,[13] P3OT,[14] and PTEBS[15]), alternating polyfluorene copolymers (such as APFO-3[16]), and low-band-gap polymers (such as PCPDTBT[17]). With regard to semiconductor NCs, CdSe has been extensively studied in HSCs for generating high PCE, although other NCs, such as CdTe, are seen as excellent candidates.[18] The main factor limiting the application of CdTe NCs in HSCs is the difficulty of finding suited polymers.

Recently, PSCs fabricated from water-soluble materials have gradually received attention given their environmental benefit.[15,19] In this scenario, the naphthalene ring is rich in electrons and naphthalene-based conjugated polymers are potentially useful in fabricating HSCs. Meanwhile, almost all of the previous HSCs are fabricated from oil-soluble materials. Many chances are missed in the absence of the construction of the methodology from water-soluble materials. Consequently, in this communication, we demonstrated the fabrication of photovoltaic devices from water-soluble CdTe NCs and poly(1,4-naphthalenevinylene) (PNV). By a primary optimization of the devices, an overall PCE of 0.86% was achieved under AM1.5G illumination.

EXPERIMENTAL SECTION

Synthesis of CdTe NCs. CdTe NCs were synthesized according to our previous report.[20] Briefly, a freshly prepared NaHTe solution was injected into a N_2-saturated $CdCl_2$ aqueous solution at pH 5.75 in the presence of 2-aminoethanethiol hydrochloride (MA) as a stabilizing agent to achieve the CdTe precursor. The molar ratio of Cd^{2+}/MA/Te was 1:2.4:0.2. The precursor solution was then subjected to a reflux that controlled the growth of the CdTe NCs. The concentration of the resulting CdTe NCs was ca. 13 mM referring to Cd^{2+}. Then, the CdTe NCs were precipitated with isopropyl alcohol at room temperature, recovered by centrifugation, and then dispersed into water to give optically clear and stable solutions. The final concentration of the CdTe NCs was 36 mg/mL, as obtained by evaporating known volumes to dryness and weighing.

Synthesis of PNV Precursor. The method for the synthesis of the PNV precursor can be found elsewhere by a slight modification.[21] Typically, polymerization was carried out in a deoxygenated aqueous solution at 0−5 °C by the reaction of 8 mL of

Received: May 17, 2011
Accepted: July 5, 2011
Published: July 05, 2011

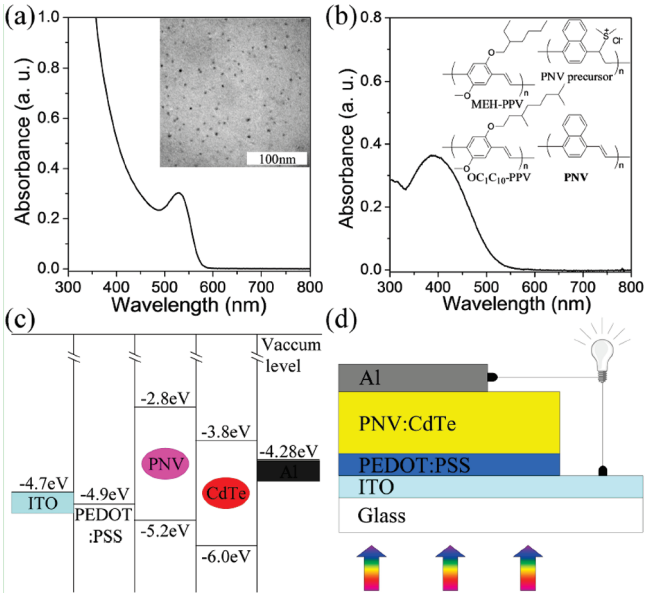

Figure 1. Absorption spectrum of 2-mercaptoethylamine-stabilized CdTe NCs (inset: TEM image of CdTe NCs) (a) and the PNV film (inset: chemical structures of the PNV precursor and PNV and conventionally used PPV derivatives) (b). Energy level diagram (c) and photovoltaic device structure (d) of PNV/CdTe NC HSCs.

1,4-naphthalenedimethylene bis(dimethylsulfonium chloride) (0.3 M) and 4 mL of sodium hydroxide (0.3 M). After the addition of sodium hydroxide, a viscous yellow solution was formed and the reaction was terminated by the addition of 0.4 M hydrochloric acid to neutralize the reaction solution. Then, the PNV precursor solution was dialyzed against deionized water for 1 week in a dialysis membrane (molecular weight cutoff at 3500) to remove the low-molecular-weight reactants and products. The final concentration of the PNV precursor solution was 4 mg/mL (referring to PNV).

Fabrication of HSCs. For device construction, a precleaned indium−tin oxide (ITO) glass was treated by O_2 plasma for 15 min. After that, a thin layer of PEDOT:PSS was foremost spin-coated onto the pretreated ITO substrate at a speed of 2000 rpm and annealed at 250 °C (which was higher than the conventional temperature around 140 °C so as to obtain a relatively sharp interface between the PEDOT:PSS layer and the photoactive layer) for 30 min in a glovebox. The aqueous solutions of the PNV precursor and CdTe NCs were directly mixed together with different volume ratios (1:0, 2:1, 1:1, 1:2, and 1:3), and the mixtures were sonicated for 30 min to realize their uniform mixing. The photoactive layer was then obtained by spin coating from a pure PNV precursor or a mixture of the PNV precursor and CdTe NCs (without filtration by a membrane) on top of the PEDOT:PSS layer at a speed of 2000or 700 rpm for 60 s in air, respectively, and subsequently annealed at 250 °C for 60 min in the glovebox to perform in situ conversion of the PNV precursor to PNV. Finally, an aluminum electrode was evaporated onto the photoactive layer in vacuo at a pressure below 10^{-5} Torr. The active area was 4 or 5 mm^2.

Characterization. UV−visible absorption spectra were acquired using a Shimadzu 3600 UV−visible−near-IR spectrophotometer. Fluorescence spectra were performed on a Shimadzu RF-5301 PC spectrophotometer with an excitation wavelength of 380 nm. Current density versus voltage ($J-V$) characteristics

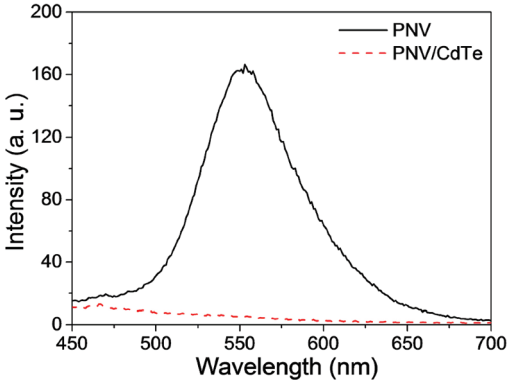

Figure 2. PL spectra of the films of pure PNV and PNV/CdTe NC blends (1:18, w/w).

were measured by a computer-controlled Keithley 2400 source meter measurement system, both in the dark and under 100 mW/cm^2 illumination with an AM1.5G filter. The incident photon-to-current efficiency (IPCE) was recorded under illumination of monochromatic light from the xenon lamp using a monochromator (Jobin Yvon, TRIAX 320) and detected by a computer-controlled Stanford SR830 lock-in amplifier with a Stanford SR540 chopper. Atomic force microscopy (AFM) micrographs were recorded in tapping mode with a Nanoscope IIIa scanning probe microscope from Digital Instruments. Transmission electron microsopy (TEM) micrographs were recorded by a Hitachi H-8100 electron microscope operating at an acceleration voltage of 200 kV.

RESULTS AND DISCUSSION

Figure 1a shows the absorption spectrum of 2-mercaptoethylamine-stabilized CdTe NCs with a diameter of 3 nm, which was calculated from the 1s−1s exciton absorption peak,[22] and the TEM image. The absorption spectrum and chemical structure of PNV are shown in Figure 1b. The maximum absorbance of a PNV film appeared at 392 nm, while the absorption onset wavelength appeared at 520 nm, from which the energy band gap of PNV was estimated to be 2.4 eV. The energy level arrangement of PNV and CdTe NCs was schematically shown in Figure 1c. The highest occupied molecular orbital (HOMO, −5.2 eV) energy level of PNV and the valence band (−6.0 eV) energy level of CdTe NCs were determined by the ultraviolet photoelectron spectroscopy (UPS) measurements of bulk thin films spin-coated on ITO. Then, the band gaps of PNV (2.4 eV) and CdTe NCs (2.2 eV) were determined by UV−visible absorption spectra of their thin films spin-coated on quartz. Finally, the lowest unoccupied molecular orbital (LUMO, −2.8 eV) energy level of PNV and the conduction band (CB, −3.8 eV) energy level of CdTe NCs were calculated from the data mentioned above, respectively. The offset between the LUMO energy level of PNV and the CB energy level of CdTe NCs was 1.0 eV, larger than the typical exciton binding energy (ca. 0.3−0.5 eV) of conjugated polymers.[31] This energy level difference could provide a sufficient driving force for direct electron transfer from photoexcited PNV to CdTe NCs. In addition, CdTe NCs were capped by small molecules of 2-mercaptoethylamine, and thus no ligand-exchange process was necessary for the device construction.[23,24] As shown in Figure 1d, photovoltaic devices were fabricated with a typical sandwich structure in the BHJ

Table 1. Photovoltaic Performance of the PNV/CdTe NC HSCs with Different PNV to CdTe NC Weight Ratios

PNV/CdTe (w/w)	J_{sc} (mA/cm^2)	V_{oc} (V)	FF	PCE (%)
1:0	−0.007	0.69	0.25	0.001
1:4.5	−2.18	0.53	0.24	0.28
1:9.0	−4.13	0.51	0.30	0.63
1:18	−6.14	0.44	0.32	0.86
1:27	−5.51	0.41	0.30	0.68

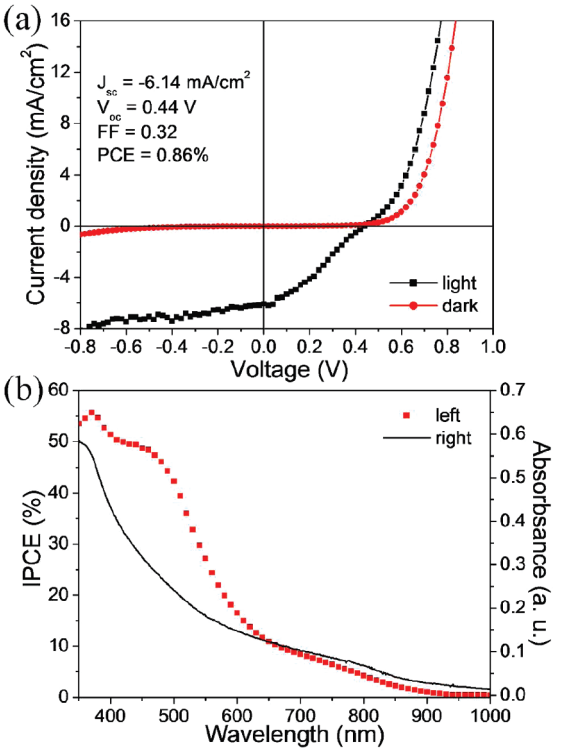

Figure 3. (a) Current density−voltage (J−V) characteristics of PNV/CdTe NC HSCs with a PNV to CdTe NCs weight ratio of 1:18. (b) IPCE as a function of the wavelength of the photovoltaic device containing PNV and CdTe NCs (1:18), coplotted with the absorption spectrum of the blend for comparison.

configuration, glass/ITO/PEDOT:PSS (55 nm)/PNV:CdTe (∼50 nm)/Al (100 nm). The devices exhibited an excellent diode behavior in the dark, with a rectification ratio of 33 at ±1 V (Figure 3a).

Photoluminescence (PL) quenching was usually used as an effective tool for evaluation of the charge-transfer efficiency in the donor−acceptor blend films.[10,25] Typically, conjugated polymers are good hole conductor materials, but recombination in the pure polymer is high because of low mobility and a short exciton diffusion length, giving rise to a strong PL signal.[26] Figure 2 shows the PL spectra of pure PNV and PNV/CdTe NC blend (1:18, w/w) films. It was observed that the PL of PNV was quenched with the addition of CdTe NCs, providing evidence of photoinduced charge transfer between PNV and CdTe NCs. Besides, complete PL quenching of PNV indicated that CdTe NCs were randomly dispersed throughout the blend film, accepting electrons from photoexcited PNV. Furthermore, the

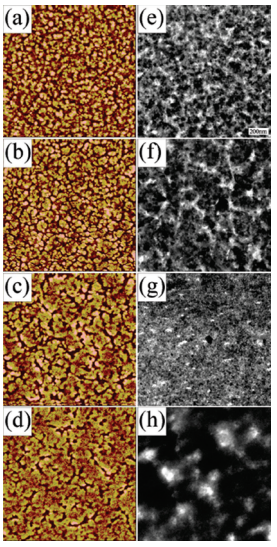

Figure 4. AFM images (size: 5 μm × 5 μm, left) and the corresponding TEM images (right) obtained from photoactive layers with different weight ratios of PNV to CdTe NCs: (a and e) 1:4.5 (rms roughness = 5.72 nm); (b and f) 1:9.0 (rms roughness = 6.55 nm); (c and g) 1:18 (rms roughness = 6.34 nm); (d and h) 1:27 (rms roughness = 4.48 nm). The height scale of the AFM images is 20 nm.

emission peak of CdTe NCs in the PL spectra was not detectable at this condition. This phenomenon might be mainly caused by the serious aggregation of CdTe NCs (Figure 4g) and ligand removal (TGA measurement, not shown) in the annealing process, which could badly decrease (or even totally quench) the PL of CdTe NCs.[22] This means that, besides charge transfer, other reasons might also lead to PL quenching. A detailed investigation is still underway.

The performance of photovoltaic devices was optimized by varying the weight ratio of PNV to CdTe NCs (Table 1). This demonstrated that the photovoltaic device made of pure PNV exhibited a PCE of only 0.001%, which was dramatically improved after the introduction of CdTe NCs into the photoactive layer. Meanwhile, with an increase of the CdTe NC content, the PCE of photovoltaic devices increased at first and then decreased after reaching a maximum PCE at a weight ratio of 1:18 of PNV to CdTe NCs. Figure 3a shows the J−V curves of the optimized photovoltaic device in the dark and under illumination of simulated AM1.5G (100 mW/cm^2). The corresponding parameters J_{sc}, V_{oc}, FF, and PCE of the device were −6.14 mA/cm^2, 0.44 V, 0.32, and 0.86%, respectively.

The IPCE spectrum of the optimized device is shown in Figure 3b, coplotted with the absorption spectrum of the corresponding blend film. One can see that the blend film has an absorption larger than 574 nm (the absorption onset wavelength of CdTe NCs; Figure 1a), which was attributed to the aggregation of CdTe NCs in the annealing process.[22] Simultaneously, it shows that there is photocurrent generation at wavelengths larger than 520 nm (the absorption onset wavelength of PNV; Figure 1b), proving that CdTe NCs were also the photoactive material in the as-prepared photovoltaic devices. Besides, J_{sc} calculated from the IPCE spectrum was 6.27 mA/cm^2, which matched very well with J_{sc} obtained from the J−V curve.

The morphology of the photoactive layer greatly contributed to the performance of π-PSCs by influencing both charge separation and transport processes.[27−32] This means that the

interfacial area between the donor and acceptor should be maximized with a regular domain size compared with the exciton diffusion length, and a continuously interpenetrating network should also be formed to favor the transport of charge carriers. To gain insight into the relationship between the morphology of the photoactive layer and the device performance, AFM and TEM were combined to investigate the morphology of blend films of PNV/CdTe NCs with different weight ratios. Figure 4 shows the AFM height images and the corresponding TEM images of PNV/CdTe NC blend films with weight ratios of 1:4.5, 1:9.0, 1:18, and 1:27, respectively. The surface of the blend films was rather smooth, and the change of the root-mean-square (rms) roughness of the films was relatively small, with a narrow range between 4.48 and 6.55 nm (Figure 4a−d).

Meanwhile, it was believed that the dark regions in the corresponding TEM images referred to the CdTe-rich domains while the light regions referred to the PNV-rich domains (Figure 4e−h). Therefore, it was observed that the CdTe-rich domains became larger with the addition of more CdTe NCs (Figure 4e−h). However, the majority of the PNV-rich domains appeared smaller than a few tens of nanometers (Figure 4e−g), which was comparable with the typical exciton diffusion length of conjugated polymers and thus would favor the exciton dissociation at the interface between PNV and CdTe NCs.[8,26] At ratios of 1:4.5 and 1:9.0, the interpenetrating network was not well developed and the CdTe-rich domains were relatively small, which were mostly isolated by the PNV-rich domains (Figure 4e,f). In contrast, at a ratio of 1:27, the excessive CdTe NCs in the blend film lead to serious aggregation of CdTe NCs. The large CdTe-rich domains (ca. 300 nm) induced the formation of large PNV-rich domains that greatly exceeded the exciton diffusion length of conjugated polymers and thus suppressed the formation of the interpenetrating network (Figure 4h). However, a continuously interpenetrating network was clearly distinguished at a ratio of 1:18 (Figure 4g). As a result, the highest FF value of 0.32 was achieved, which indicated the balanced transport of charge carriers.[28,33,34] Besides, the larger aggregate of CdTe-rich domains would narrow the band gap of CdTe NCs and thus diminish the offset between the HOMO energy level of PNV and the CB energy level of CdTe NCs, which might partially explain the decrease of V_{oc} as the weight ratio of PNV to CdTe NCs changed from 1:4.5 to 1:27 (Table 1).[22,35−37]

CONCLUSIONS

In summary, we have successfully fabricated a HSC from water-soluble CdTe NCs and PNV. On the basis of the AFM and TEM studies, we suggested that a continuously interpenetrating network formed by simply adjusting the ratio of PNV to CdTe NCs, which led to a maximum PCE of 0.86% at the optimized ratio. Our results revealed that PNV was a promising π-conjugated polymer, and meanwhile water was an alternative to the conventional organic solvent in fabricating HSCs. The current effort will soundly promotes the development of HSCs in a simple and environmentally friendly way.

AUTHOR INFORMATION

Corresponding Author

*Fax: +86-431-85193423. E-mail: byangchem@jlu.edu.cn.

ACKNOWLEDGMENT

This work was supported by NSFC (Grants 20974038, 20921003, and 50973039) and the Special Project from MOST of China.

REFERENCES

(1) Tang, C. W. *Appl. Phys. Lett.* **1986**, *48*, 183–185.
(2) Sariciftci, N. S.; Smilowitz, L.; Heeger, A. J.; Wudl, F. *Science* **1992**, *258*, 1474–1476.
(3) Chen, J. W.; Cao, Y. *Acc. Chem. Res.* **2009**, *42*, 1709–1718.
(4) Chen, H.-Y.; Hou, J. H.; Zhang, S. Q.; Liang, Y. Y.; Yang, G. W.; Yang, Y. L.; Yu, P.; Wu, Y.; Li, G. *Nat. Photonics* **2009**, *3*, 649–653.
(5) Martínez-Ferrero, E.; Albero, J.; Palomares, E. *J. Phys. Chem. Lett.* **2010**, *1*, 3039–3045.
(6) Yu, G.; Gao, J.; Hummelen, J. C.; Wudl, F.; Heeger, A. J. *Science* **1995**, *270*, 1789–1791.
(7) Halls, J. J. M.; Walsh, C. A.; Greenham, N. C.; Marseglia, E. A.; Friend, R. H.; Moratti, S. C.; Holmes, A. B. *Nature* **1995**, *376*, 498–500.
(8) Günes, S.; Neugebauer, H.; Sariciftci, N. S. *Chem. Rev.* **2007**, *107*, 1324–1338.
(9) Wang, Y.; Herron, N. *Chem. Phys. Lett.* **1992**, *200*, 71–75.
(10) Greenham, N. C.; Peng, X. G.; Alivisatos, A. P. *Phys. Rev. B* **1996**, *54*, 17628–17637.
(11) Sun, B. Q.; Marx, E.; Greenham, N. C. *Nano Lett.* **2003**, *3*, 961–963.
(12) Zhou, Y.; Li, Y. C.; Zhong, H. Z.; Hou, J. H.; Ding, Y. Q.; Yang, C. H.; Li, Y. F. *Nanotechnology* **2006**, *17*, 4041–4047.
(13) Huynh, W. U.; Dittmer, J. J.; Alivisatos, A. P. *Science* **2002**, *295*, 2425–2427.
(14) Lee, H.; Yoon, S. W.; Kim, E. J.; Park, J. *Nano Lett.* **2007**, *7*, 778–784.
(15) Qiao, Q. Q.; McLeskey, J. T. *Appl. Phys. Lett.* **2005**, *86*, 153501.
(16) Wang, P.; Abrusci, A.; Wong, H. M. P.; Svensson, M.; Andersson, M. R.; Greenham, N. C. *Nano Lett.* **2006**, *6*, 1789–1793.
(17) Dayal, S.; Kopidakis, N.; Olson, D. C.; Ginley, D. S.; Rumbles, G. *Nano Lett.* **2010**, *10*, 239–242.
(18) Zhou, Y. F.; Eck, M.; Krüger, M. *Energy Environ. Sci.* **2010**, *3*, 1851–1864.
(19) Mwaura, J. K.; Pinto, M. R.; Witker, D.; Ananthakrishnan, N.; Schanze, K. S.; Reynolds, J. R. *Langmuir* **2005**, *21*, 10119–10126.
(20) Zhang, H.; Liu, Y.; Zhang, J. H.; Wang, C. L.; Li, M. J.; Yang, B. *J. Phys. Chem. C* **2008**, *112*, 1885–1889.
(21) Antoun, S.; Gagnon, D. R.; Karasz, F. E.; Lenz, R. W. *J. Polym. Sci., Part C: Polym. Lett.* **1986**, *24*, 503–509.
(22) Yu, W. W.; Qu, L. H.; Guo, W. Z.; Peng, X. G. *Chem. Mater.* **2003**, *15*, 2854–2860.
(23) Seo, J.; Kim, W. J.; Kim, S. J.; Lee, K.-S.; Cartwright, A. N.; Prasad, P. N. *Appl. Phys. Lett.* **2009**, *94*, 133302.
(24) Lek, J. Y.; Xi, L. F.; Kardynal, B. E.; Wong, L. H.; Lam, Y. M. *ACS Appl. Mater. Interfaces* **2011**, *3*, 287–292.
(25) Beek, W. J. E.; Wienk, M. M.; Janssen, R. A. J. *Adv. Funct. Mater.* **2006**, *16*, 1112–1116.
(26) Coakley, K. M.; McGehee, M. D. *Chem. Mater.* **2004**, *16*, 4533–4542.
(27) Shaheen, S. E.; Brabec, C. J.; Sariciftci, N. S.; Padinger, F.; Fromherz, T.; Hummelen, J. C. *Appl. Phys. Lett.* **2001**, *78*, 841–843.
(28) Van Duren, J. K. J.; Yang, X. N.; Loos, J.; Bulle-Lieuwma, C. W. T.; Sieval, A. B.; Hummelen, J. C.; Janssen, R. A. J. *Adv. Funct. Mater.* **2004**, *14*, 425–434.
(29) Peet, J.; Kim, J. Y.; Coates, N. E.; Ma, W. L.; Moses, D.; Heeger, A. J.; Bazan, G. C. *Nat. Mater.* **2007**, *6*, 497–500.
(30) Oosterhout, S. D.; Wienk, M. M.; Bavel, S. S. V.; Thiedmann, R.; Koster, L. J. A.; Gilot, J.; Loos, J.; Schmidt, V.; Janssen, R. A. J. *Nat. Mater.* **2009**, *8*, 818–824.
(31) Slota, J. E.; He, X. M.; Huck, W. T. S. *Nano Today* **2010**, *5*, 231–242.
(32) Graham, K. R.; Mei, J. G.; Stalder, R.; Shim, J. W.; Cheun, H.; Steffy, F.; So, F.; Kippelen, B.; Reynolds, J. R. *ACS Appl. Mater. Interfaces* **2011**, *3*, 1210–1215.

(33) Mihailetchi, V. D.; Xie, H. X.; Boer, B. D.; Koster, L. J. A.; Blom, P. W. M. *Adv. Funct. Mater.* **2006**, *16*, 699–708.
(34) Mikroyannidis, J. A.; Kabanakis, A. N.; Sharma, S. S.; Sharma, G. D. *Adv. Funct. Mater.* **2011**, *21*, 746–755.
(35) Brabec, C. J.; Cravino, A.; Meissner, D.; Sariciftci, N. S.; Fromherz, T.; Rispens, M. T.; Sanchez, L.; Hummelen, J. C. *Adv. Funct. Mater.* **2001**, *11*, 374–380.
(36) Scharber, M. C.; Mühlbacher, D.; Koppe, M.; Denk, P.; Waldauf, C.; Heeger, A. J.; Brabec, C. J. *Adv. Mater.* **2006**, *18*, 789–794.
(37) Perez, M. D.; Borek, C.; Forrest, S. R.; Thompson, M. E. *J. Am. Chem. Soc.* **2009**, *131*, 9281–9286.